Robust Dirac-Cone Band Structure in the Molecular Kagome Compound (EDT-TTF-$CONH_2)_6[Re_6Se_8(CN)_6]$

Cite as:
Carlsson, S., Zorina, L., Allan, D. R., Attfield, J. P., Canadell, E., & Batail, P. (2013). Robust Dirac-Cone Band Structure in the Molecular Kagome Compound (EDT-TTF-$CONH_2$)$_6$[$Re_6Se_8(CN)_6$]. *Inorganic Chemistry*, 52(6), 3326-3333.

Manuscript received: 21/12/2012; Article published: 22/02/2013

Robust Dirac-Cone Band Structure in the Molecular Kagome Compound (EDT-TTF-$CONH_2$)$_6$[$Re_6Se_8(CN)_6$]**

Sandra Carlsson,[1] Leokadiya Zorina,[2,3] David R. Allan,[1,4] J. Paul Attfield,[1,*] Enric Canadell[5,*] and Patrick Batail[2,*]

[1]EaStCHEM, School of Chemistry and Centre for Science at Extreme Conditions, Joseph Black Building, University of Edinburgh, West Mains Road, Edinburgh, EH9 3JJ, UK.

[2]Laboratoire MOLTECH-Anjou, CNRS & Université d'Angers, 2 Boulevard Lavoisier, 49045 Angers, France.

[3]Institute of Solid State Physics RAS, 142432 Chernogolovka, MD, Russia.

[4]Diamond Light Source Ltd., Didcot, OX11 0DE UK.

[5]Institut de Ciència de Materials de Barcelona (ICMAB-CSIC), Campus de la UAB, E-08193, Bellaterra, Spain.

[*]Corresponding authors; J.P.A. e-mail: j.p.attfield@ed.ac.uk; E.C. e-mail: canadell@icmab.es; P.B. e-mail: patrick.batail@univ-angers.fr

[**]This work was supported by EPSRC, the Leverhulme Trust, the Royal Society UK, INTAS Grant 04-83-4001, RFBR-CNRS Grant 12-03-91059, CNRS and ANR France, and the Spanish Ministerio de Economía y Competitividad (Projects FIS2009-1271-C04-03, CSD 2007-00041, and SAB2011-0047).

Supporting information:

Further experimental details and structure refinement results; two tables summarizing single crystal X-ray results, seven figures showing atom labeling for EDT-TTF-CONH2, a diffraction data frame at 0.4 GPa, intermolecular contacts, Le Bail fits, variation of intermolecular hydrogen bond lengths with pressure, definition of intradimer distances and angle, their pressure dependences; and X-ray crystallographic files in CIF format for refined structures. This material is available free of charge via the Internet at http://pubs.acs.org

Abstract:

$(EDT\text{-}TTF\text{-}CONH_2)_6[Re_6Se_8(CN)_6]$ is a molecular solid with $R\bar{3}$ space group symmetry and has the remarkable feature of exhibiting hybrid donor layers with a kagome topology which sustain metallic conductivity. We report a detailed study of the structural evolution of the system as a function of temperature and pressure. This rhombohedral phase is maintained on cooling down to 220 K or up to 0.7 GPa pressure, beyond which a symmetry-breaking transition to a triclinic $P\bar{1}$ phase drives a metal to insulator transition. Band structures calculated from the structural data lead to a clear description of the effects of temperature and pressure on the structural and electronic properties of this system. Linear energy dispersion is calculated at the zero-gap Fermi level where valence and conduction bands touch for the rhombohedral phase. $(EDT\text{-}TTF\text{-}CONH_2)_6[Re_6Se_8(CN)_6]$ thus exhibits a regular (right circular) Dirac-cone like that of graphene at the Fermi level, which has not been reported previously in a molecular solid. The Dirac-cone is robust over the stability region of the rhombohedral phase, and may result in exotic electronic transport and optical properties.

■ INTRODUCTION

Subtle details and variations of the band structure often lie at the origin of unconventional properties of solids. For example, interest in zero-gap materials with linear energy dispersion at the Fermi level, has been boosted following the discovery of efficient ways to isolate single graphene layers. In these zero-gap materials, the valence and conduction bands touch at single points in the Brillouin zone and the effective mass of the carriers is extremely low because of the linear energy dispersion at the Fermi level. Consequently, the carriers may be described through the relativistic massless Dirac equation leading to exotic electronic properties.[1] The topology of the energy dispersion around these special points is described as a Dirac-cone. Dirac-cones are essential to the unusual electronic properties of graphene[2,3,] and topological insulators such as Bi_2Se_3.[4] However, there are still relatively few extended materials that exhibit this feature, and Dirac-cones are almost unknown in molecular solids. α-$(BEDT\text{-}TTF)_2I_3$ (where BEDT-TTF stands for bis(ethylenedithio)tetrathiafulvalene) is reported to show a Dirac-cone under applied pressure,[5] but the cone is tilted unlike the regular (right circular) Dirac-cone in high-symmetry materials such as graphene.

Molecular conductors[6] are typically composed of stacks of planar, functional π-conjugated molecules which crystallize in low-symmetry space groups (monoclinic or triclinic)[7] and thus have complex band structures.[8] However, highly symmetric molecular packings are sometimes observed and can lead to simple structural topologies and band structure features of fundamental interest. $(EDT\text{-}TTF\text{-}CONH_2)_6[Re_6Se_8(CN)_6]$ (hereafter referred to as Compound **1**) is notable example, where the building units are not discrete molecules but rather secondary structures with a $\bar{3}$ point symmetry held together in a six-fold N–H···N≡C hydrogen bonded motif.[9,10] Compound **1** was found to crystallise in a layered rhombohedral lattice with a kagome topology, which is known in extended inorganic lattices such as $[NH_4]_2[C_7H_{14}N][V_7O_6F_{18}]$,[11] but is a remarkable feature for a molecular metal. Compound **1**

displays a low temperature metal-insulator transition accompanied by a symmetry-breaking structural transition.[9]

In this paper we report subsequent structural studies that have established the pressure and temperature stability region for the metallic rhombohedral phase of Compound **1**, and have provided accurate models for the rhombohedral and the triclinic, insulating phases. Complementary variable pressure transport measurements will be reported elsewhere.[12] Accurate crystal structure models are important for band structure calculations, and we show that the Fermi level of the metallic phase occurs at the K-point of the two-dimensional hexagonal Brillouin zone such that the system behaves as a zero-gap material with a remarkable linear energy dispersion. Compound **1** thus represents the first reported example of a molecular material with a regular (right circular) Dirac-cone band structure.

■ EXPERIMENTAL SECTION

X-ray diffraction studies.

Ambient pressure single crystal studies at temperatures of 100-295 K were performed using a laboratory 4-circle diffractometer with monochromatized MoK_α-radiation (wavelength λ = 0.71073Å) at the Université d'Angers. High pressure experiments were performed at the Daresbury Synchrotron Radiation Source, Warrington, UK, with samples in a diamond anvil cell. Powder data up to 4.8 GPa from station 9.5 (λ = 0.44374 Å) and single crystal data up to 1.8 GPa from station 9.8 (λ = 0.6751 Å) were collected at room temperature. Further experimental details and results are shown in Supporting Information.

Computational details. The tight-binding band structure calculations[13] were of the extended Hückel type. A modified Wolfsberg-Helmholtz formula was used to calculate the non-diagonal $H_{\mu\nu}$ values.[14] All valence electrons were taken into account in the calculations and the basis set consisted of Slater-type orbitals of double-ζ quality for C, N and O 2s and 2p, S 3s and 3p and of single-ζ quality for H. The ionization potentials, contraction coefficients and exponents were taken from previous work.[15,16]

■ RESULTS AND DISCUSSION

Variable temperature crystal structure.

The room-temperature rhombohedral phase of Compound **1**, $(EDT\text{-}TTF\text{-}CONH_2)_6[Re_6Se_8(CN)_6]$, has $R\bar{3}$ space group symmetry. The distinctive feature is the presence of hybrid donor-anion layers with a kagome topology (Figure 1).[9] The edges of the kagome lattice hexagons and triangles are decorated with centrosymmetric dimers of EDT-TTF-$CONH_2$ molecules and the hexagonal cavities are filled by $[Re_6Se_8(CN)_6]^{4-}$ molecular cluster anions. The molecular packing is held together by numerous hydrogen-bonded contacts and other intermolecular interactions.

Upon cooling, Compound **1** undergoes a transition at 220 K to a triclinic $P\bar{1}$ phase. Lattice parameters obtained while lowering the temperature of a single crystal are shown in the rhombohedral cell setting in Figure 2. The cell parameters *a* and *b* undergo a similar contraction at temperatures below the transition while *c* significantly increases, illustrating the distortion of the kagome lattice from rhombohedral to triclinic symmetry (Figure 3). No discontinuities in the cell parameters or volume are observed as the temperature is lowered, suggesting that the transition is second order.

All EDT-TTF-$CONH_2$ dimers are symmetry equivalent in the high temperature rhombohedral structure, but three dimers labeled **A**, **B** and **C** on Figure 3 become nonequivalent as the symmetry is reduced to triclinic at the transition. As noted previously,[9] these show a charge order as $\mathbf{A}^{\bullet+}$ and $\mathbf{C}^{\bullet+}$ are spin-1/2 radical dimers while $\mathbf{B}^{2+}$ dimers are spin paired. The detailed mechanism for this change is revealed by the accurate crystal structure determinations in this study (Figure 4): molecules in dimer **B** rotate around their short in-plane molecular axes in a direction opposite to that of the rotation of molecules in **A** and **C**. Deviations from the room temperature positions of the molecular planes amount to 2-4º at 100 K. As a result, the pattern of overlap within dimer **B** differs from that within **A** and **C**. A charge calculation using an empirical formula based on the bond lengths in TTF-type organic donors[17] at 100 K gives values of +0.65, +0.91, and +0.59 respectively for molecules within **A**, **B** and **C** dimers, which confirms the charge ordering. The localization of an extra hole on dimer $\mathbf{B}^{2+}$ brings the molecules closer in this dimer, as illustrated by the interplanar separations of 3.45(2),

3.38(1) and 3.41(2) Å for **A**, **B** and **C**, respectively, and S···S orbital overlap interactions become noticeably stronger in $\mathbf{B}^{2+}$ than in $\mathbf{A}^{\bullet+}$ and $\mathbf{C}^{\bullet+}$ (Figure 4c).

Conformational order of ethylene fragments in the EDT-TTF-$CONH_2$ units is also observed at temperatures below the phase transition. The ethylene fragment is disordered between two conformations in a 0.57:0.43 ratio in the 295 K rhombohedral structure, but full ordering is observed at 100 K with dimers **A** and **C** having a different conformation to **B**, as shown in Figure 4a. This creates two strong intermolecular $C_{ethylene}$–H···O hydrogen bonds in **B** dimers that are absent for **A** and **C**. Further information about the intermolecular contacts is given as Supporting Information.

High pressure crystal structure

Synchrotron X-ray powder data from Compound **1** were analyzed with the GSAS software package.[18] The complexity of the structure precluded refinement of the crystal structure, or of cell parameters for the triclinic phase. Instead, the Le Bail method[19] (of fitting freely-varying peak intensities) was used to refine the rhombohedral lattice parameters a and α and the Lorentzian LY peak-shape coefficient, which describes strain-broadening of the diffraction peaks, at each pressure. Typical profile plots are shown in Supporting Figure S4, and the pressure variations of the refined parameters are shown in Figure 5. The cell parameters and volume decrease with increasing pressure while the strain broadening increases. Although no structural change is evident from visual inspection of the diffraction profiles, a discontinuity in all the fitted parameters near 0.7 GPa (Fig. 5) evidences a structural transition, which is confirmed by the single crystal data below. No further transitions are evident up to ~4 GPa. At the highest pressures an unphysical increase in cell volume and decrease in LY is apparent. This indicates that the parameter fitting is no longer reliable due to excessive pressure broadening of the diffraction peaks, as shown in Supporting Figure S4.

Diffraction data from a single crystal of Compound **1** in a diamond anvil cell were collected at ambient and 0.4, 0.8, 1.2 and 1.8 GPa pressures. The crystal symmetry was found to be rhombohedral at 0 and 0.4 GPa and triclinic at 0.8 to 1.8 GPa, showing that a single crystal to single crystal phase transition had occurred between 0.4 and 0.8 GPa. This is consistent with the 0.7 GPa transition

pressure estimated from the powder study. The structures were refined using the rhombohedral $R\bar{3}$ and triclinic $P\bar{1}$ models for the low and high pressure phases respectively. Refinement details are given in Supporting Information.

The pressure variation of the lattice constants of Compound **1** around the rhombohedral-triclinic transition (Figure 6) is comparable to the temperature dependence shown in Figure 2. The *c*-axis is the least compressible in the triclinic phase, and the relative magnitudes of the three cell angles above 0.7 GPa are the same as observed upon cooling at ambient pressure. The effect of pressure on the intradimer contacts is found to be similar to that of cooling. Changes in the intradimer S…S distances in Figure 7 show that the **A** and **C** pairs are less similar to each other at high pressure than in the low temperature, ambient pressure structures in Figure 5. However, further analysis based on the intermolecular C-C distances and angles within the dimers (shown in Supporting Information) demonstrates that **A** and **C** dimers are still distinct from **B**, confirming that the charge order of the triclinic phase is maintained to at least 1.8 GPa pressure.

Electronic structure calculations. The new variable temperature and pressure crystal structures presented above represent a clear improvement with respect to the previous results,[9] and thus have been used to investigate the detailed band structure of Compound **1**. As shown in Figures 1 and 3 and discussed above, all EDT-TTF-$CONH_2$ pairs in the kagome lattice of the ambient, rhombohedral phase are equivalent, whereas inequivalent **AA**, **BB** and **CC** intermolecular interactions occur within dimers, and across the closest interdimer **AB**, **AC** and **BC** contacts. The calculated values of the intermolecular interaction energies[20] $|\beta_{HOMO\text{-}HOMO}|$ for the different donor···donor pairs are reported in Table 1. These show that the donors are strongly dimerized and the interactions within dimers are sizeable and much greater than the interpair interactions. The localization of an additional bonding electron in the **B**-dimer leads to a substantial enhancement of $|\beta_{HOMO\text{-}HOMO}|$ for this dimer in the triclinic charge ordered structure. The interaction energies also reflect the increasing disparity between the **A** and **C** pairs with increasing pressure that is seen in the S…S contacts in Figure 5.

The calculated band structure for the donor layers at room temperature and ambient pressure is shown in Figure 8. The six HOMO-based bands split in two well-separated groups as expected for a lattice of strongly dimerized units. Each group of bands has the shape expected for a one-orbital per site kagome lattice with degeneracies at the K and Γ points.[21] The lower set of bands, which is built from the bonding combination of the HOMOs of the dimer, is completely filled. The upper set of bands, built from the antibonding combination of the HOMOs of the dimers, contains only two electrons and since the dispersion of these bands is quite sizeable, the system is expected to be metallic, in keeping with conductivity measurements.[9] It is notable that with this band filling, the Fermi level occurs at the K point of the 2D hexagonal Brillouin zone. Since the interlayer interactions, either direct or indirect through the anions, are associated with hydrogen bonding and these interactions do not implicate the donors' HOMO, this feature is preserved in the 3D electronic structure. Thus, compound **1** is predicted to be a zero-gap material with Dirac-cone type linear energy dispersion, as observed in graphene.[2,3] No molecular metals exhibiting a regular (right circular) Dirac-cone in the band structure have previously been reported, furthermore Compound **1** exhibits this feature at ambient temperature and pressure. As mentioned in the Introduction, α-ET_2I_3 has been proposed to exhibit a tilted Dirac-cone but only under pressure, [2] and in this system the zero-gap does not occur at a high-symmetry point of the Brillouin zone (i.e. the zero-gap is due to accidental degeneracy) and the shape of the Dirac-cone is highly dependent of the structural details which may be modified by pressure and temperature. In contrast, the Dirac-cone of Compound **1** occurs at the K symmetry point of the 2D Brillouin zone and a regular Dirac-cone exists as long as the rhombohedral structural symmetry is preserved. Hence the carriers in the metallic phase may be described through the relativistic massless Dirac equation and Compound **1** should exhibit exotic transport, magnetotransport and optical properties. Quantum electronic effects such as Shubnikov–De Haas and other oscillations are most evident at low temperatures, so the lower stability limit of 220 K for the rhombohedral phase of Compound **1** may be a practical limitation for some properties, and exploration of derivatives or analogous systems will be worthwhile to extend molecular Dirac-cone phases to lower temperatures.

The band structure for the triclinic phase of Compound **1** at ambient pressure and 100 K is shown in Figure 9. To compare the band structure with that of the rhombohedral phase, one must take into account that the path Γ →K→M in Figure 8 is equivalent to Γ →M in Figure 9, and Γ →M in Figure 8 corresponds to Γ →X and Γ →Y in Figure 9. The main differences concerning the upper set of bands are that the flat band is strongly raised in energy, and that the degeneracy at the K-point in Figure 8 now leads to a small gap in Figure 9. Otherwise the shape of the bands is quite similar. The lower band of the upper set appears to have become separated from the adjacent one, however, an exploration of the Brillouin zone around this point shows that the two lower bands are separated by a tiny indirect gap of only 2 meV which is irrelevant at the temperature of the transition and lies within the error limits of the calculation. Note also that the global dispersion of the two lower bands has decreased from Figure 8 to Figure 9, which is consistent with electronic localization. The upper flat band is concentrated in the **B** dimers whereas the lower pair of bands is delocalized over the two remaining donors (**A** and **C**). The upper flat band has been pushed up in energy because the transition from rhombohedral to triclinic symmetry is associated with a sliding of the donors in dimer **B** such that the two molecules become half-eclipsed leading to a much stronger HOMO···HOMO interaction.[9] The overlaps for the two other dimers are almost unaffected.

The activated conductivity at temperatures below the transition is associated with the localization of the two electrons in dimers **A** and **C**, driven by the dimerization in **B** that shifts the carriers towards those dimers, and the narrowing of bands from **A** and **C**, which leads to carrier localization to decrease electronic repulsions. These effects are consistent with the relatively large $|\beta_{HOMO\text{-}HOMO}|$ values for the **AC** interdimer interaction shown in Table 1. The results confirm the scenario proposed previously[9] in order to explain the failure of an initial band theory approach, which on the basis of a lower quality crystal structure led to the prediction of a clear band gap between the second and third bands from the top in Figure 9, and a non-activated spin susceptibility at temperatures below the transition.

The calculated band structures for the crystal structures obtained under 0.8, 1.2 and 1.8 GPa are very similar to that of Figure 9 and thus are not described in detail. The band gaps between the second and third bands from the top are 1.2, 13.6 and 32 meV, respectively. The accuracy of these values is

questionable because of the uncertainties in the high pressure crystal structures, in particular in the lengthening of the central C=C bond of the donor which correlates with development of positive charge. However, the similarity of band structures and the $|\beta_{HOMO-HOMO}|$ values in Table 1 reveal that pressure essentially brings about the same features as thermal contraction; an increase in the degree of dimerization within **B** dimers and weaker interactions within the other two. In conclusion, the change from non-activated to activated conductivity is brought about by the concerted action of the change in structural symmetry, molecular displacements and electron localization.

■ CONCLUDING REMARKS

$(EDT\text{-}TTF\text{-}CONH_2)_6[Re_6Se_8(CN)_6]$ has an unusually high ($R\bar{3}$) space group symmetry for a molecular solid at room temperature and ambient pressure. This gives rise to a kagome topology in the hybrid donor layers which supports metallic conductivity. The properties of this phase are maintained on cooling down to 220 K or at room temperature up to 0.7 GPa pressure, beyond which a symmetry-breaking transition to a triclinic $P\bar{1}$ phase drives a metal to insulator transition. Accurate structural data have been used to calculate the band structure of the donor layers, leading to a clear description of the effects of temperature and pressure on this system. The change from non-activated to activated conductivity is brought about by the concerted action of structural symmetry-breaking, molecular displacements and electron localization. A remarkable property of the band structure of the rhombohedral phase is that it exhibits a regular (right circular) Dirac-cone at the Fermi level which is robust provided the rhombohedral symmetry is maintained. $(EDT\text{-}TTF\text{-}CONH_2)_6[Re_6Se_8(CN)_6]$ is the first molecular solid reported to exhibit this unusual feature, and detailed physical characterization will be required to observe possible exotic electronic transport and optical properties.

■ AUTHOR INFORMATION

Corresponding Authors

* j.p.attfield@ed.ac.uk, canadell@icmab.es, patrick.batail@univ-angers.fr

Author Contributions

The manuscript was written through contributions of all authors. All authors have given approval to the final version of the manuscript.

■ ASSOCIATED CONTENT

Supporting Information. Further experimental details and structure refinement results; two tables summarising single crystal x-ray results, seven figures showing atom labeling for EDT-TTF-$CONH_2$, a diffraction data frame at 0.4 GPa, intermolecular contacts, Le Bail fits, variation of intermolecular hydrogen bond lengths with pressure, definition of intradimer distances and angle, their pressure dependences; and X-ray crystallographic files in CIF format for refined structures. This material is available free of charge via the Internet at http://pubs.acs.org.

■ ACKNOWLEDGMENT

This work was supported by EPSRC, the Leverhulme Trust, the Royal Society UK, INTAS Grant 04-83-4001, RFBR-CNRS grant 12-03-91059, CNRS and ANR France, and the Spanish Ministerio de Economía y Competitividad (Projects FIS2009-1271-C04-03, CSD 2007-00041 and SAB2011-0047).

■ ABBREVIATIONS

EDT-TTF, ethylenedithiotetrathiafulvalene.

■ REFERENCES

(1) Castro Neto, A. H.; Guinea, F.; Peres, N. M. R.; Novoselov, K. S.; Geim, A. K. *Rev. Mod. Phys*. **2009**, *81*, 109-162.

(2) Novoselov, K. S.; Geim, A. K.; Morozov, S. V.; Jiang, D.; Katsnelson, M. I.; Grigorieva, I. V.; Dubonos, S. V.; Firsov, A. A., *Nature*, 2005, **438**, 197-200.

(3) (a) Montambaux, G.; Piéchon, F.; Fuchs, J.-N.; Goerbig, M. O. *Phys. Rev. B* **2009**, *80*, 153412. (b) Montambaux, G.; Fuchs, J.-N.; Goerbig, M. O.; Piéchon, F. *Eur. Phys. J. B* **2009**, *72*, 509-520.

(4) Xia,Y.; Qian, D.; Hsieh, D.; Wray, L.; Pal, A.; Lin, H.; Bansil, A.; Grauer, D.; Hor, Y. S.; Cava, R. J.; Hasan, M. Z. *Nature Physics* **2009,** *5,* 398 – 402.

(5) Katayama, S.; Kobayashi, A.; Suzumura, Y. *J. Phys. Soc. Jpn*. **2006**, *75*, 054705:1-054705:6.

(6) For a comprehensive overview of the chemistry and physics of molecular conductors, see: *Chem. Rev.* **2004**, *104(11)*, 4887-5782.

(7) Fourmigué, M.; Batail, P. *Chem. Rev.* **2004**, 104 (11), 5379-5418.

(8) (a) Rousseau, R.; Gener, M.; Canadell, E. *Adv. Funct. Mater.* **2004**, *14*, 201-214; (b) Canadell, E.; Doublet, M.-L.; Iung, C. *Orbital Approach to the Electronic Structure of Solids*, Oxford University Press, 2012.

(9) Baudron, S. A.; Batail, P.; Coulon, C.; Clérac, R.; Canadell, E.; Laukhin, V.; Melzi, R.; Wzietek, P.; Jérome, D.; Auban-Senzier, P.; Ravy, S. *J. Am. Chem. Soc.* **2005**, *127*, 11785-11797.

(10) For a discussion, relying on concepts of soft matter physics, of the ability to optimize packing in high-symmetry space groups of typically low point-group symmetry (charged) molecules, see: (a) Horner, M. J.; Holman, K. T.; Ward, M. D. *J. Am. Chem. Soc.* **2007**, *129*, 14640-14660; see also: (b) Perruchas, S.; Boubekeur, K.; Canadell, E.; Misaki, Y.; Auban-Senzier, P.; Pasquier, C.; Batail, P. *J. Am. Chem. Soc.* **2008**, *130*, 3335-3348.

(11) Aidoudi, F. H.; Aldous, D. W.; Goff, R. J.; Slawin, A. M. Z.; Attfield, J. P.; Morris, R. E.; Lightfoot, P. *Nat. Chem.*, **2011**, *3*, 801–806.

(12) Variable pressure transport data and the observation of a metal-insulator transition at ca. 0.5 GPa will be reported by Jacimovic, Forro et al. in a future paper.

(13) Whangbo, M.-H.; Hoffmann, R. *J. Am. Chem. Soc*. **1978**, *100*, 6093-6098.

(14) Ammeter, J. H.; Bürgi, H.-B.; Thibeault, J.; Hoffmann, R. *J. Am. Chem. Soc.* **1978**, *100*, 3686-3692.

(15) Pénicaud, A.; Boubekeur, K.; Batail, P.; Canadell, E.; Auban-Senzier, P.; Jérome, D. *J. Am. Chem. Soc*., **1993**, *115*, 4101-4112.

(16) Baudron, S. A.; Avarvari, N.; Canadell, E.; Auban-Senzier, P.; Batail, P. *Chem. Eur. J.* **2004**, *10*, 4498-4511.

(17) Guionneau, P.; Kepert, C. J.; Bravic, G. ; Chasseau, D.; Truter, M. R. ; Kurmoo, M.; Day, P. *Synth. Met.* **1997**, *86*, 1973-1974.

(18) Larson, A.C.; Von Dreele, R.B. "General Structure Analysis System (GSAS)", Los Alamos National Laboratory Report LAUR 86-748 (1994).

(19) Le Bail, A.; Duroy, H.; Fourquet, J.L. *Mater. Res. Bull.* **1988** *23*, 447-452.

(20) Whangbo, M.-H.; Williams, J. M.; Leung, P. C. W.; Beno, M. A.; Emge, T. J.; Wang, H. H. *Inorg. Chem*. **1985**, *24*, 3500-3502.

(21) Johnston, R. L.; Hoffmann, R. *Polyhedron* **1990**, *9*, 1901-1911.

Table 1. Absolute values of the EDT-TTF-$CONH_2$ HOMO···HOMO intermolecular interaction energies $|\beta_{HOMO\text{-}HOMO}|$ (eV) in Compound **1** for the various intermolecular interactions as a function of pressure and temperature. The first two entries are for the rhombohedral ($R\bar{3}$) phase where all molecules are symmetry-equivalent, and the others correspond to the triclinic low temperature phase ($P\bar{1}$) structure.

P (GPa)	*T* (K)	**AA**	**BB**	**CC**	**AB**	**AC**	**BC**
0	295		0.6823			0.1234	
0.4	295		0.7062			0.1287	
0	100	0.6525	0.9261	0.6751	0.1214	0.1078	0.1557
0.8	295	0.5005	0.7982	0.5224	0.1108	0.1164	0.0825
1.2	295	0.5324	0.7836	0.5924	0.0928	0.1020	0.0697
1.8	295	0.5022	0.8210	0.5801	0.0775	0.0849	0.0400

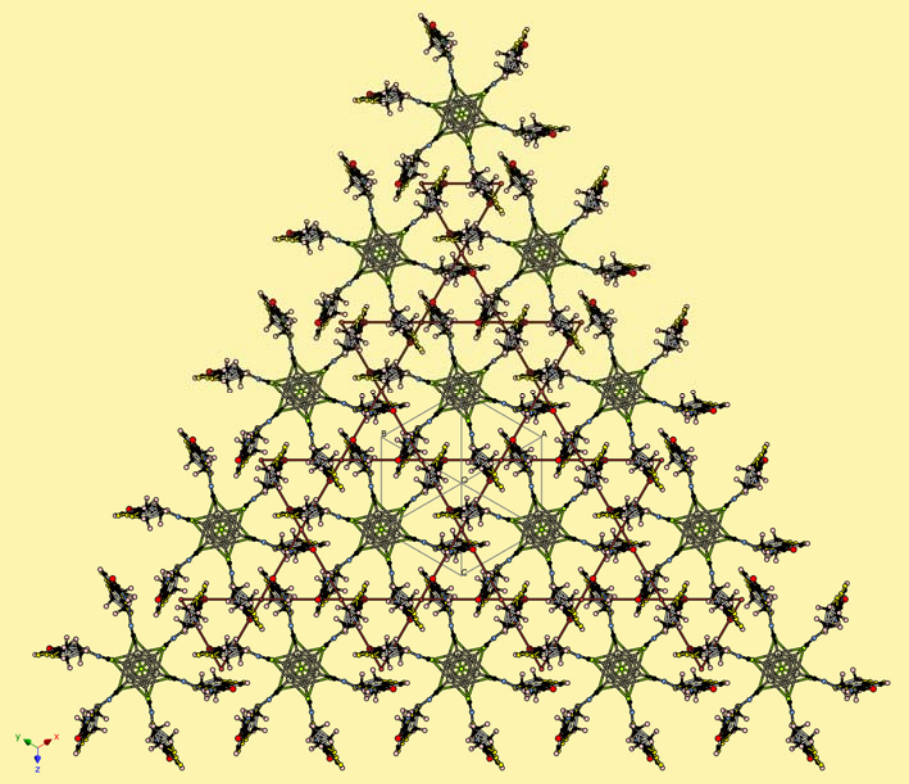

Figure 1. A single kagome layer of the rhombohedral structure of Compound **1** at 230 K.

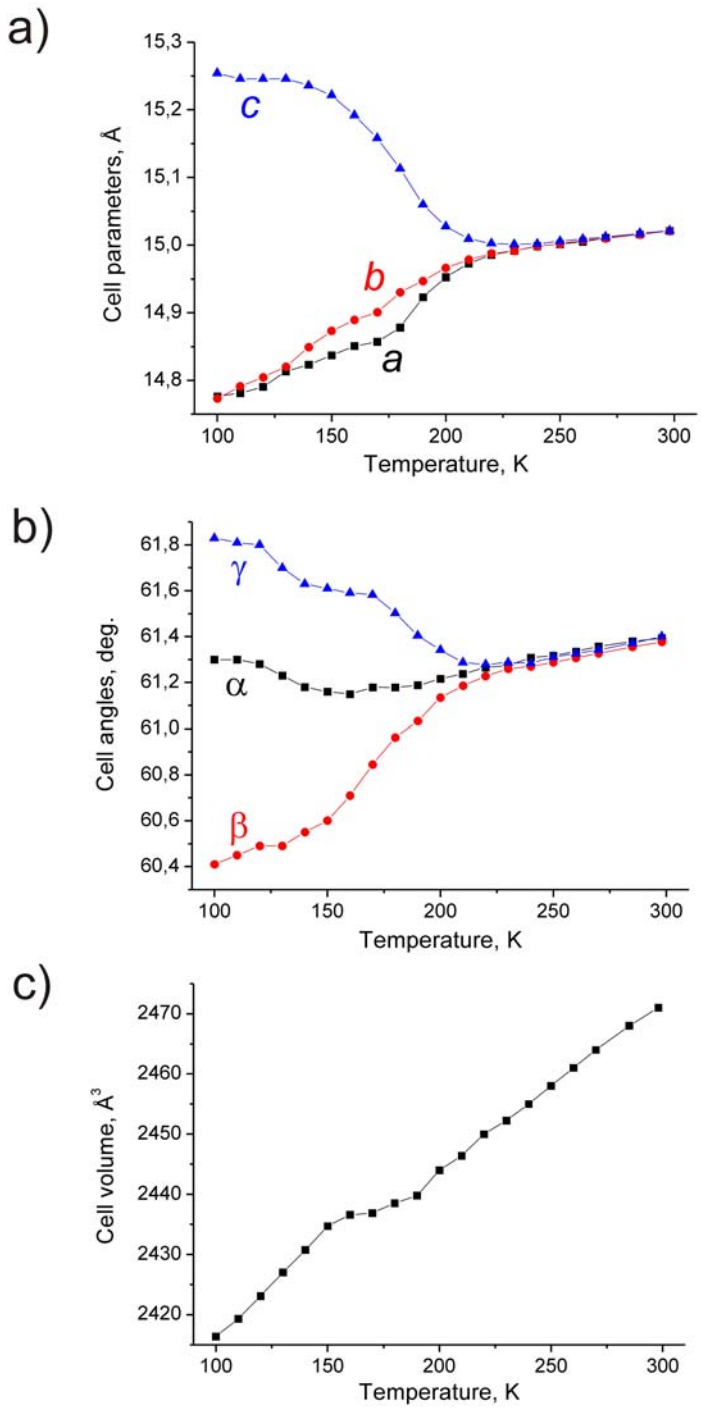

Figure 2. Changes in the unit cell parameters ((a) axis-lengths, (b) cell angles and (c) volume; rhombohedral setting) upon lowering the temperature of a single crystal of Compound **1**.

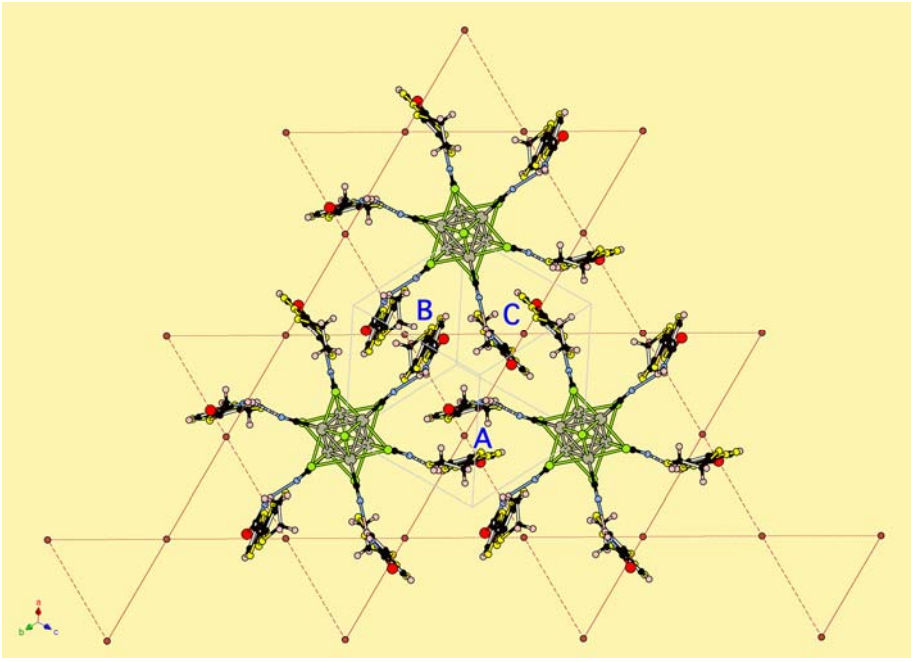

Figure 3. Distortion of a single kagome layer of Compound **1** in the 100 K, ambient pressure crystal structure, showing inequivalent dimers **A**, **B** and **C**.

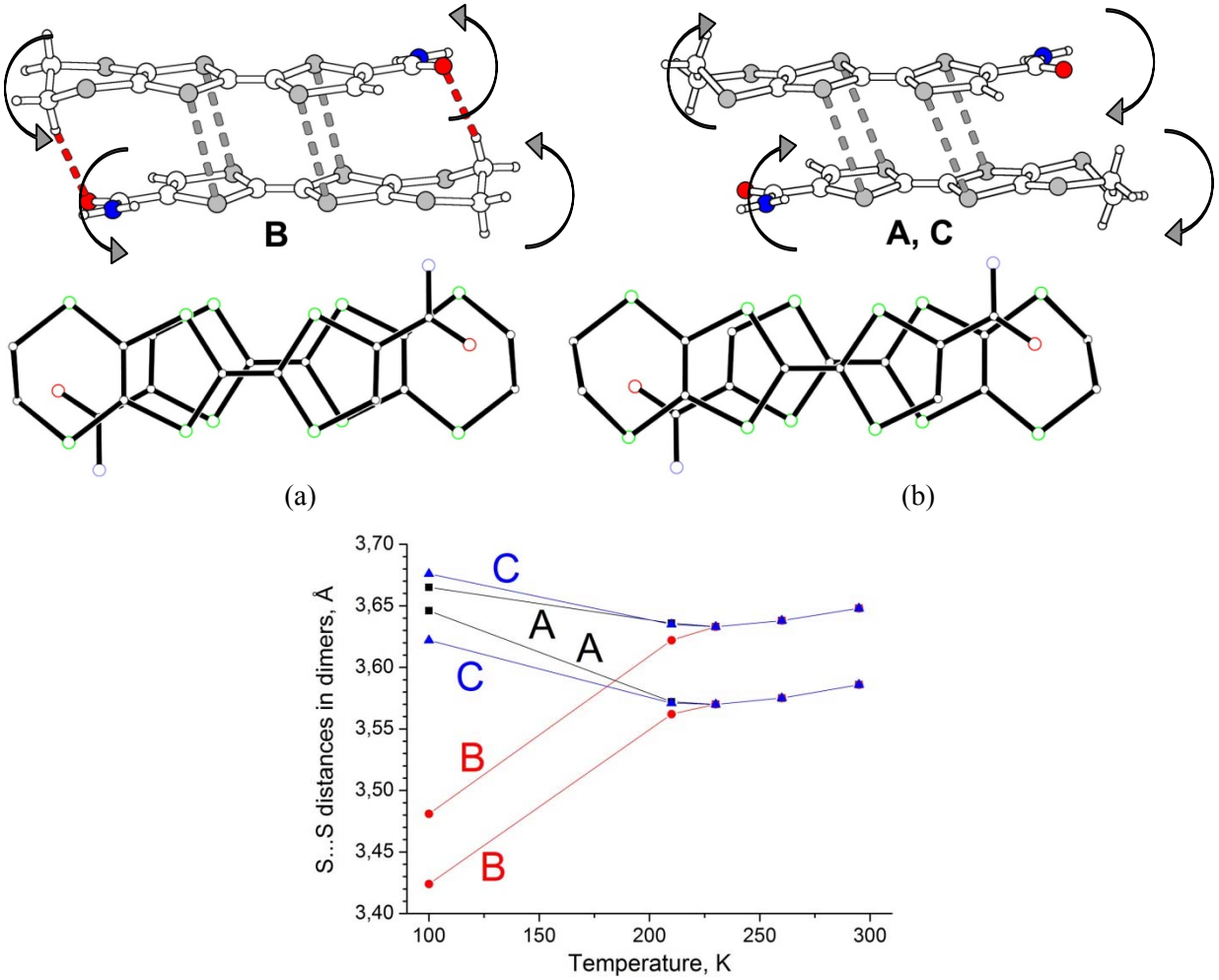

Figure 4. Rearrangements in the two types of dimer in Compound **1** on cooling through the rhombohedral to trinclinic structural transition. Side and top views of (a) $\mathbf{B}^{2+}$ dimers and (b) $\mathbf{A}^{\bullet+}$ and $\mathbf{C}^{\bullet+}$ dimers are shown with arrows indicating the rotation of each molecule around its short in-plane axis. (c) Temperature variation of S···S distances in the dimers.

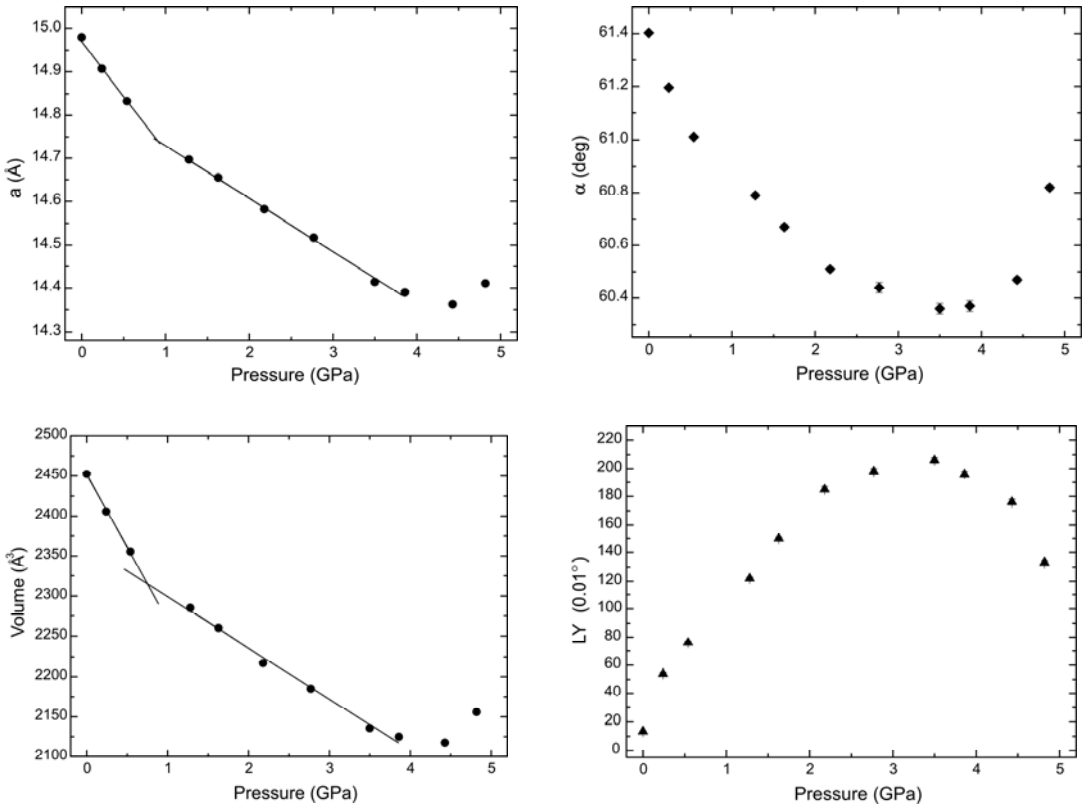

Figure 5. Plots of fitted rhombohedral lattice parameters and volume and the Lorentzian strain broadening coefficient with pressure for Compound **1** at room temperature.

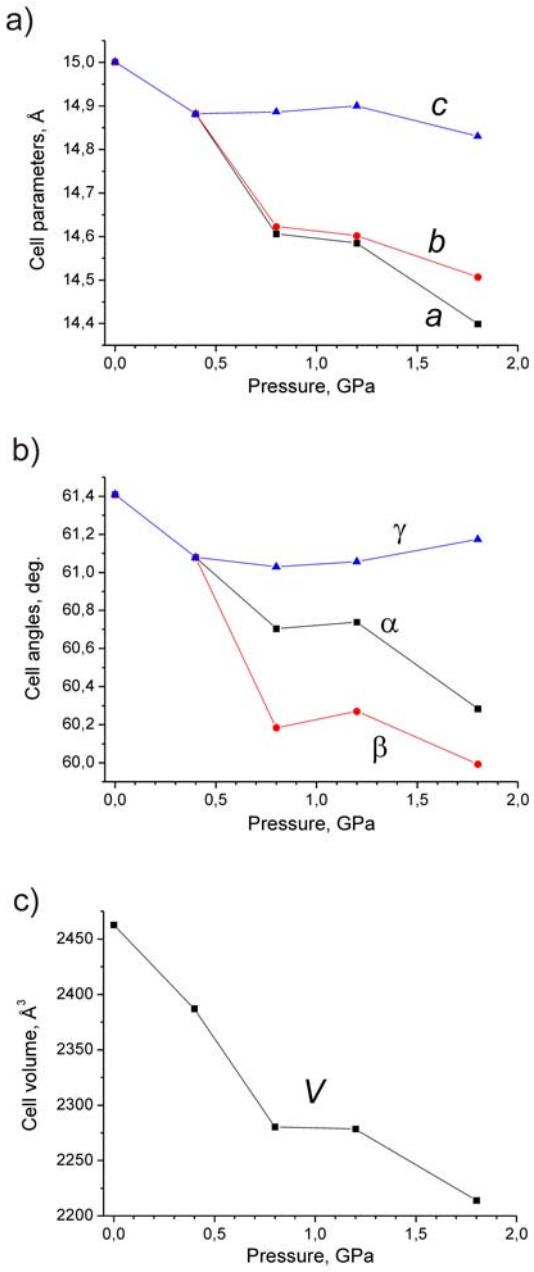

Figure 6. Changes in the unit cell parameters ((a) axis-lengths, (b) cell angles and (c) volume; rhombohedral setting) with pressure for a single crystal of Compound **1** at room temperature.

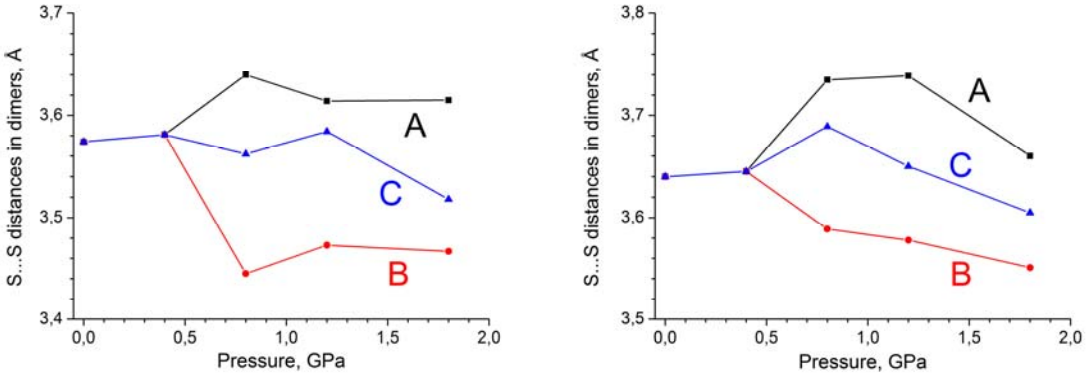

Figure 7. Pressure variations of the two intradimer S…S distances in Compound **1**, shown for inequivalent dimers **A**, **B** and **C** as defined by Figures 3 and 4 in the triclinic phase.

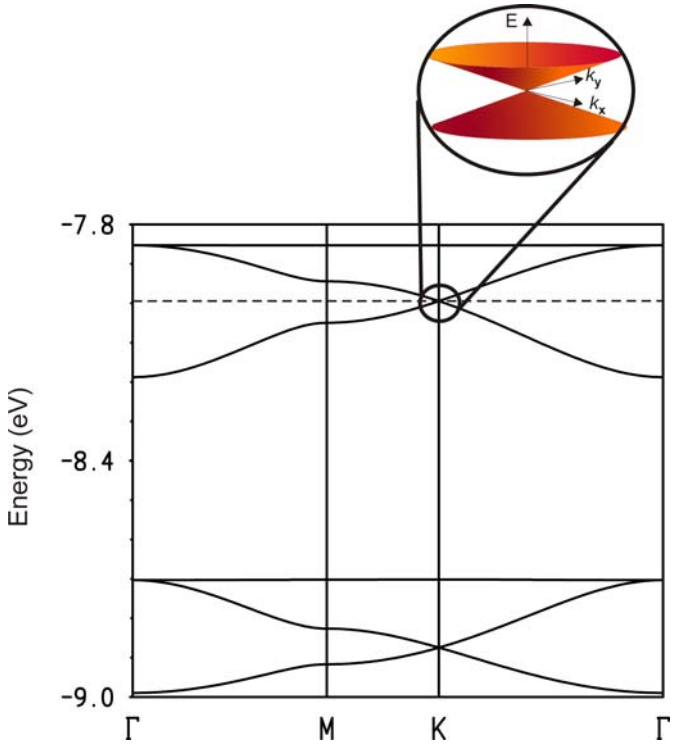

Figure 8. Calculated band structure for the donor layers of (EDT-TTF-$CONH_2$)$_6$[$Re_6Se_8(CN)_6$] in the ambient temperature and pressure rhombohedral phase**,** where the dashed line refers to the Fermi level and Γ = (0, 0), M = (a_1*/2, 0) and K = (a_1*/3, a_2*/3). The magnification around the K point is a schematic representation of the band dispersion around this point, i.e. the Dirac-cone.

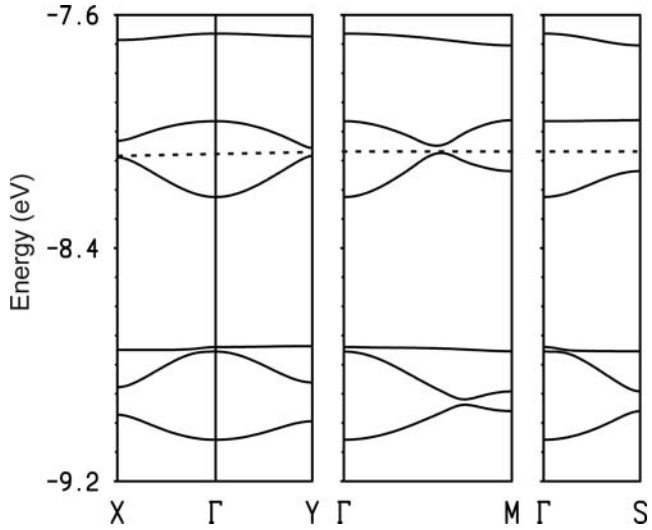

Figure 9. Calculated band structure for the donor layers of (EDT-TTF-$CONH_2$)$_6$[$Re_6Se_8(CN)_6$] in the triclinic phase at 100 K and ambient pressure**,** where Γ = (0, 0), X = (a_1*/2, 0), Y = (0, a_2*/2), M = (a_1*/2, a_2*/2) and S = (-a_1*/2, a_2*/2). The dashed line refers to the highest occupied level of the system.

TOC figure

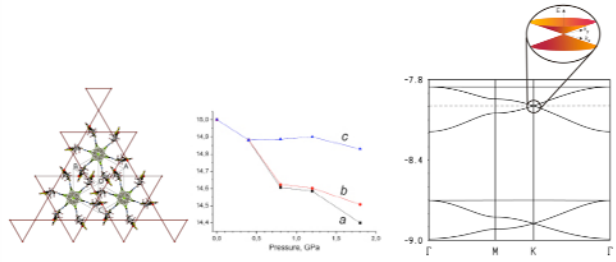

TOC text;

The molecular solid (EDT-TTF-$CONH_2$)$_6$[$Re_6Se_8(CN)_6$] has hybrid donor layers with a kagome topology that maintain rhombohedral symmetry on cooling down to 220 K or up to 0.7 GPa pressure, beyond which a metal to insulator transition and lattice distortion occur. Band structure calculations reveal a Dirac-cone at the Fermi level, like that of graphene, which may result in exotic electronic properties.